applied sciences

MDPI

Article

Aspect Ratio Evolution in Embedded, Surface, and Corner Cracks in Finite-Thickness Plates under Tensile Fatigue Loading

Jesús Toribio *, Juan-Carlos Matos and Beatriz González

Fracture & Structural Integrity Research Group (FSIRG), University of Salamanca (USAL), E.P.S., Campus Viriato, Avda. Requejo 33, 49022 Zamora, Spain; jcmatos@usal.es (J.-C.M.); bgonzalez@usal.es (B.G.)

* Correspondence: toribio@usal.es; Tel.: +34-980-545-500 (ext. 3659); Fax: +34-980-545-002

Academic Editor: César M. A. Vasques

Received: 28 April 2017; Accepted: 6 July 2017; Published: 21 July 2017

Abstract: This article deals with the computational modelling of the fatigue crack aspect ratio evolution in embedded, surface, and corner cracks located in finite-thickness plates under tensile fatigue. The approach is based on the Paris law for fatigue propagation and an expression for the stress intensity factor (SIF) provided by Newman and Raju. Numerical results indicate that the crack path develops in such a manner that all flaws tend to reach similar aspect ratios, i.e., a *preferential crack path does exist* along which there is a one-to-one relationship between the aspect ratio and the relative crack depth (a sort of *master curve* in the matter of fatigue crack path evolution). Such a reference curve corresponds to that of a very superficial initial flaw with almost circular shape. The convergence (quicker or slower approach between fatigue crack paths starting from different initial defects) is higher for surface flaws than for corner cracks, and quicker for the latter than for embedded discontinuities. Corner defects increase their size faster than surface cracks, and the latter do the same quicker than the embedded ones.

Keywords: numerical modelling; finite-thickness cracked plate; Paris law; preferential crack path; fatigue life

1. Introduction

The stress intensity factor (SIF) in cracked plates of finite thickness is very useful in fracture mechanics and damage tolerance approaches. SIF solutions for this geometry were provided by Newman and Raju in a classical paper [1] and more recently by other authors [2–4]. In plates with a surface crack under tension loading, the maximum SIF is reached at the crack center when the aspect ratio is lower than 0.6 and at the border when it is higher [5]. For embedded cracks, the maximum SIF is achieved near the free surface [6]. In the case of corner cracks, the highest values of the SIF occurred at the free surface along the width direction for cracks in which the depth is higher than the other dimension and at the free surface along the thickness direction for cracks in which the depth is lower than the other dimension [7].

The crack front evolution for semielliptical cracks in plates was numerically analyzed [8–13] through the Paris law [14] and the SIF, sometimes taking into account hypothetical crack closure effects on the SIF value [15] or using the root mean square (RMS) SIF (an integrated average of the SIF) [16], considering only two points or a set of points over the crack front and assuming a pre-defined crack shape or with no shape constraints. A new finite element simulation technique using fatigue crack growth circles needs a small number of crack front increments [17], while the conventional method requires several hundred increments to get accurate results. In [18], a review is presented on 3D-FE adaptive remeshing techniques for crack growth modeling.

The existence of free surfaces has a great influence on crack advancement. Cracks tend to propagate reaching a constant SIF along their front (iso-*K*), but the free surface prevents this phenomenon [19]. Surface cracks in plates tend to propagate following a preferential cracking path [8,13] which depends on the kind of loading applied on the specimen (tension or bending). The crack aspect ratio for a semi-elliptical surface crack in a pipe subjected to internal pressure is similar to that of a plate in tension [20]. For the same conditions, corner cracks grow quicker than surface flaws, and surface flaws more rapidly than embedded cracks [21]. In the case of surface or corner cracks near semicircular notches or holes, results of the SIF exhibit higher values when the ratio of the notch (or hole) radius to the plate thickness increases [22–24] so that cracks emanating from stress areas such as notches or holes advance by fatigue at a higher rate near the stress concentrator than they do far from it.

This article deals with the computational modelling of the fatigue crack aspect ratio evolution in embedded, surface, and corner cracks located in finite-thickness plates under tensile fatigue. The approach is based on the Paris law for fatigue propagation and an expression for the SIF provided by Newman and Raju. To fill the gap existing in the scientific literature, a comparison of the preferential propagation path, the dimensionless SIF evolution, and the number of cycles required for propagation between the three case studies needs to be performed.

2. Numerical Modelling

A computer program in Java programming language was developed to study the propagation path of elliptical embedded cracks, semi-elliptical surface cracks, and quarter-elliptical corner cracks on the cross section of a plate (Figure 1) subjected to fatigue (cyclic) loading in the form of remote uniform tension (under Mode-I loading conditions). The plate has a finite thickness; the height and the width are large enough to avoid any influence of the boundary on the SIF value.

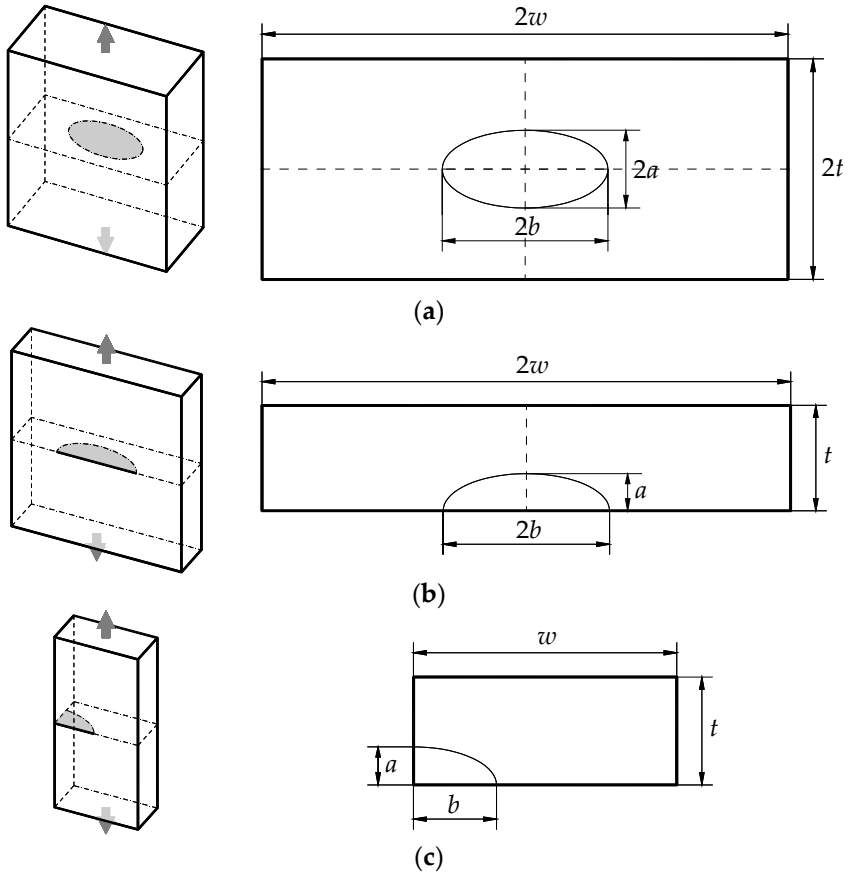

Figure 1. Scheme of a finite-thickness plate with: (**a**) an elliptical embedded crack; (**b**) a semi-elliptical surface crack; (**c**) a quarter-elliptical corner crack.

The crack front was characterized as an ellipse of semiaxes a (crack depth) and b (crack length), see Figure 1, and a specific point p over the crack front is determined by the angular parameter ϕ as a function of the relationship between the semiaxes a and b (Figure 2).

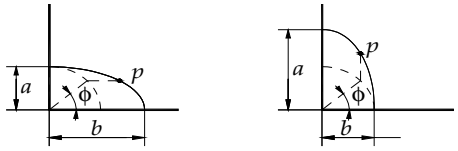

(**a**) (**b**)

Figure 2. Angle ϕ defining a specific point p over the crack front: (**a**) $a/b \leq 1$; (**b**) $a/b > 1$.

2.1. Stress Intensity Factor (SIF)

The SIFs used were those obtained by Newman and Raju [1] by a three-dimensional (3D) finite element analysis and the nodal-force method. These authors adjusted their results to an equation that calculates the SIF K:

$$K = \sigma\sqrt{\frac{\pi a}{Q}}F \tag{1}$$

where the function Q is the shape factor for an ellipse (given by the square of the complete elliptic integral of the second kind) and depends on the aspect ratio a/b as follows:

For $\frac{a}{b} \leq 1$,

$$Q = 1 + 1.464\left(\frac{a}{b}\right)^{1.65} \tag{2}$$

For $\frac{a}{b} > 1$,

$$Q = 1 + 1.464\left(\frac{b}{a}\right)^{1.65} \tag{3}$$

F is a function of the parameters: a/b (crack aspect ratio, see Figure 1), a/t (relative crack depth, see Figure 1), and ϕ the angle representing the specific position at the crack front (see Figure 2). The function F is different depending on if the crack is embedded, surface, or corner-type and is calculated by means of the expression,

$$F = \left[M_1 + M_2\left(\frac{a}{t}\right)^2 + M_3\left(\frac{a}{t}\right)^4\right]gf_\phi \tag{4}$$

where the parameters M_1, M_2, M_3, g, and f_ϕ are obtained through the equations in Appendix A.

In Table 1 the ranges are given of the variables a/b, a/t, and ϕ for which the Equations in Appendix A are valid for the calculation of the SIF in an embedded, surface, or corner crack placed in a plate subjected to tensile cyclic loading.

Table 1. Applicability ranges for the equations by Newman and Raju [1].

Parameters	Configuration		
	Embedded Crack	**Surface Crack**	**Corner Crack**
a/b	0 to ∞	0 to 2	0.2 to 2
a/t	<1.25 (a/b + 0.6) if $0 \leq a/b \leq 0.2$ <1 if $a/b > 0.2$		<1
ϕ	$-\pi$ to π	0 to π	0 to $\pi/2$

2.2. Crack Front Evolution

The basic hypothesis of this modelling is the assumption that the crack front can be characterized as an ellipse (see characteristic dimensions in Figure 1) and that fatigue propagation takes place in a direction perpendicular to such a front, following the Paris law [14],

$$\frac{\mathrm{d}a}{\mathrm{d}N} = C\Delta K^{\mathrm{m}} \tag{5}$$

The fatigue process uncertainties eliminate any advantages of using a fatigue crack growth law that is more complex and has more material parameters than the Paris law, cf. [25].

To discretize the crack front, modelled in an elliptical way, it was divided into z segments of equal length using the Simpson's rule. Subsequently, each of the points i was moved perpendicularly to the crack front, in accordance with the Paris law, so that the maximum crack increase, $\Delta a(\max)$, corresponding to the point of the maximum SIF (maximum parameter F, $F(\max)$) was kept constant during the whole computation. From this maximum increase $\Delta a(\max)$ and the SIF, the advance Δa_{i} of each of the front points can be obtained as:

$$\Delta a_{\mathrm{i}} = \Delta a(\max)\left[\frac{F_{\mathrm{i}}}{F(\max)}\right]^{\mathrm{m}} \tag{6}$$

The new points, fitted by the method of least squares to minimize the error, form a new ellipse, as described elsewhere [26], so that the crack advance progress is repeated iteratively up to reaching the required relative crack depth. The ranges of the used variables were as follows: $0.2 \le a/b \le 2$, $0.02 < a/t < 1$, and $0 \le \phi \le \pi/2$ (only a quarter of the ellipse was studied in the three cases due to the symmetry exhibited by both the embedded and the surface cracks). Parameters z and $\Delta a(\max)$ were determined by a study of convergence to find out the most adequate values to obtain a reliable result ($z = 12$ and $\Delta a(\max) = 0.00001t$).

The number of cycles N required for fatigue crack propagation can be calculated, from the Paris law given by Equation (5), with the expression,

$$N = \frac{1}{C\Delta\sigma^{\mathrm{m}}\pi^{\mathrm{m}/2}}\int_{a_0}^{a_{\mathrm{f}}}\frac{Q^{\mathrm{m}/2}}{F^{\mathrm{m}}a^{\mathrm{m}/2}}\mathrm{d}a \tag{7}$$

where a_0 and a_{f} are, respectively, the initial and final crack depth.

The dimensionless number of cycles n necessary for fatigue crack propagation is obtained through the following expression (on the basis of the trapezoidal rule),

$$n = \int_{a_0}^{a_{\mathrm{f}}}\frac{Q^{\mathrm{m}/2}}{F^{\mathrm{m}}a^{\mathrm{m}/2}t^{(2-\mathrm{m})/2}}\mathrm{d}a \tag{8}$$

3. Numerical Results

Figures 3–5 show the crack propagation (a/b-a/t) curves for embedded, surface, and corner cracks placed in a plate under tension, with different initial geometry defined by $(a/t)_0$ and $(a/b)_0$, and for distinct materials represented by the exponent m of the Paris law (values $m = 2$, 3, and 4 were used in this paper). In one of the curves of Figure 3a, a dot is used to signal the initial geometry of the crack ($(a/t)_0 = 0.1$, $(a/b)_0 = 0.2$) and arrows are placed over the curve to indicate the sense of growth.

The crack advance from different initial geometries tends towards a *preferential propagation path*, it being consistent with previous research [8]. In the present paper, such a preferential path is linked to a very shallow initial crack with quasi-circular front, the convergence (closeness between curves) being higher for surface cracks than for corner flaws, and higher for the latter than for those embedded in the plate. Cracks growing from initial geometries $(a/b)_0 = \{1, 1.5, \text{and } 2\}$ exhibit quicker convergence than those with initial geometries $(a/b)_0 = \{0.2 \text{ and } 0.5\}$. In addition, the convergence is

faster: (i) as the m-exponent of the Paris law increases, (ii) as the initial crack depth $(a/t)_0$ diminishes, and (iii) as the initial crack geometry ($(a/t)_0$, $(a/b)_0$) becomes closer to the preferential cracking path.

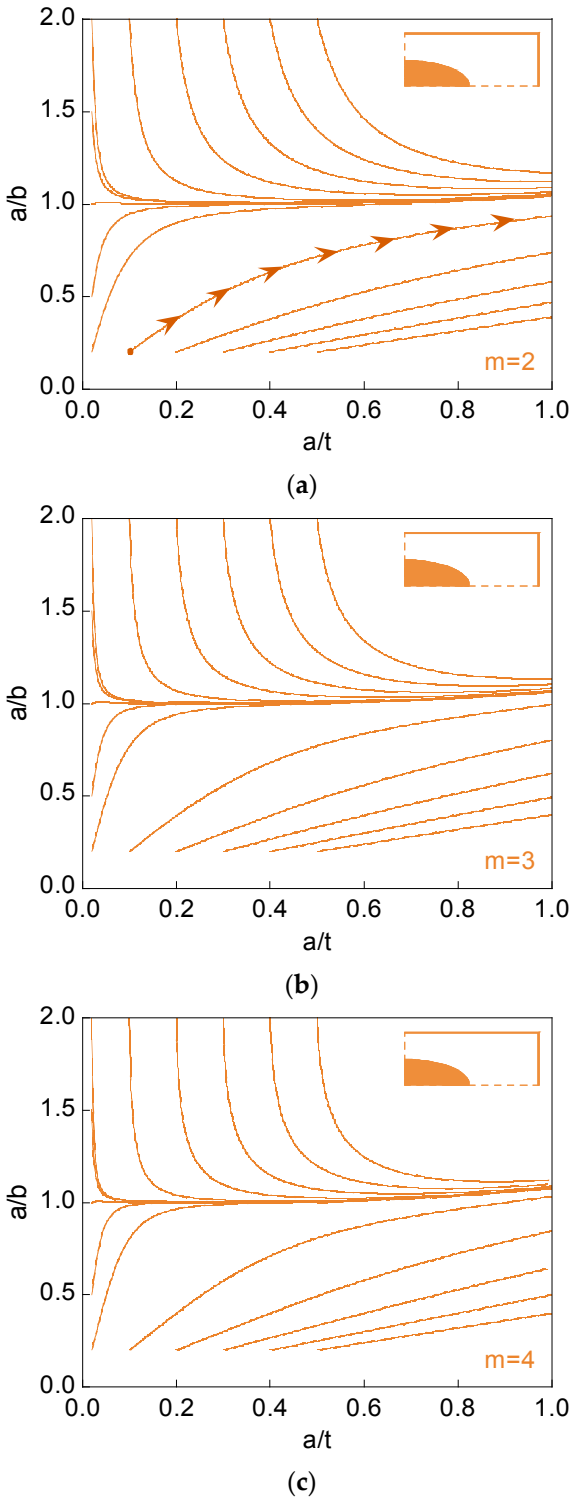

Figure 3. Aspect ratio evolution with relative crack depth (propagation path) for embedded cracks: (**a**) $m = 2$; (**b**) $m = 3$; (**c**) $m = 4$.

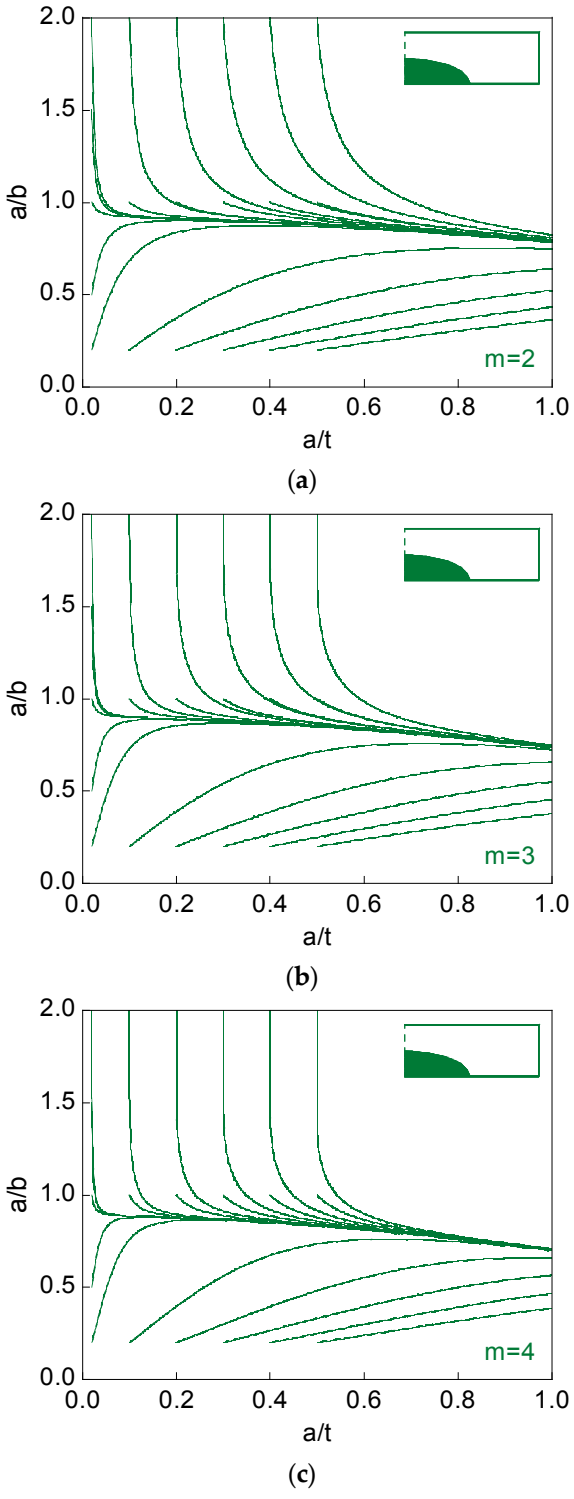

Figure 4. Aspect ratio evolution with relative crack depth (propagation path) for surface cracks: (**a**) $m = 2$; (**b**) $m = 3$; (**c**) $m = 4$.

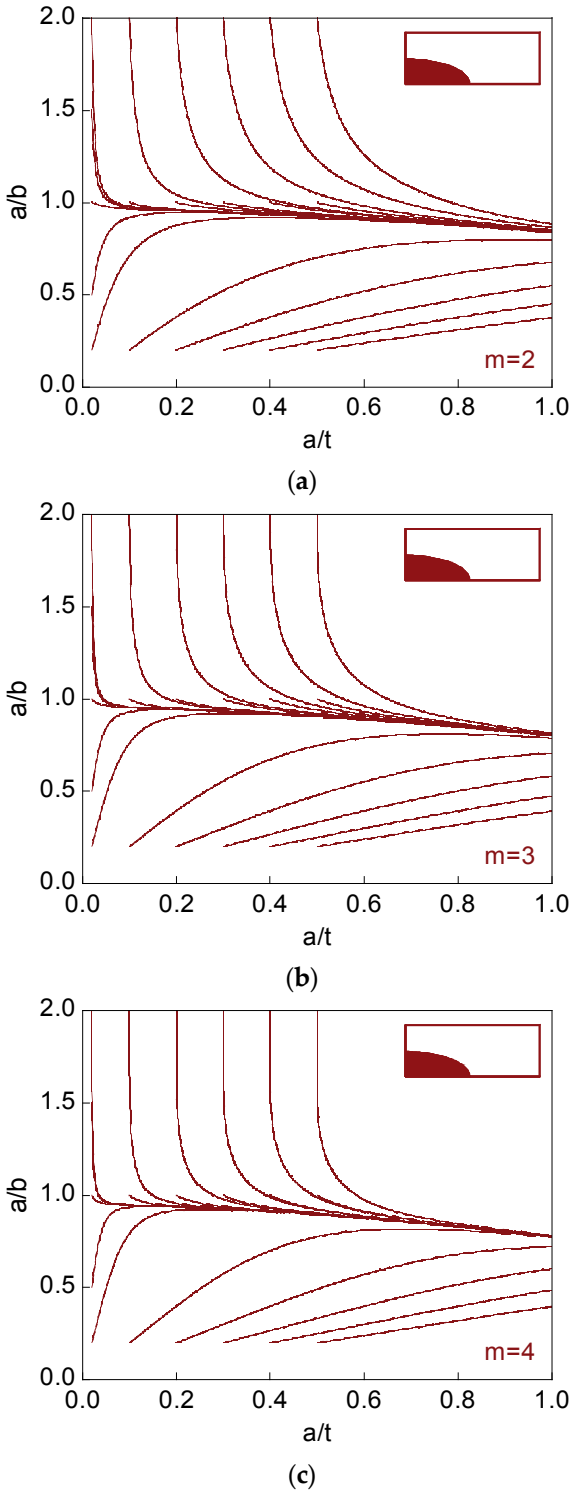

Figure 5. Aspect ratio evolution with relative crack depth (propagation path) for corner cracks: (**a**) $m = 2$; (**b**) $m = 3$; (**c**) $m = 4$.

4. Discussion

Figure 6 shows the preferential propagation path for the three analyzed configurations and for Paris exponents m = 2, 3, and 4. For embedded cracks, the preferential path exhibits values of the aspect ratio higher than 1, they being close to 1 up to a depth a/t = 0.4, and slightly increases with the relative crack depth for a/t > 0.4. For surface and corner cracks such a preferential path presents aspect ratios lower than 1, which diminish along with the relative crack depth. The Paris coefficient m raises the preferential plot a/b-a/t for embedded cracks when a/t > 0.4 and lowers it for surface and corner flaws (this trend being valid for the whole range of a/t).

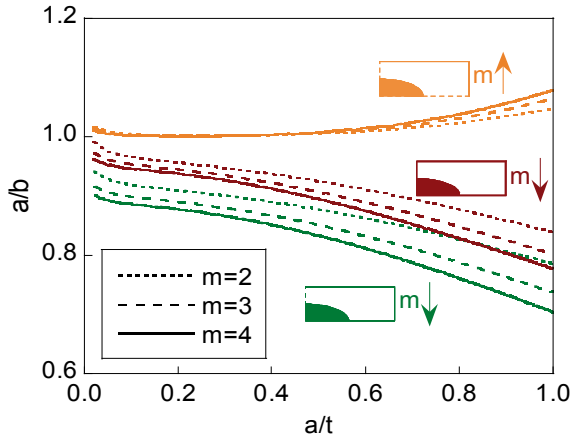

Figure 6. Preferential propagation paths. (The arrows indicate the direction in which the curves are moved with the increase of the Paris m exponent).

The embedded defects in infinite solids under fatigue tend towards an iso-K state [27], but the free surface (front, back, and lateral side) of the plate ensures that the iso-K state is not reached for the preferential crack path.

In the matter of the preferential cracking path, Figure 7 plots the dimensionless SIF $K/(\sigma(\pi a)^{1/2})$ at three points of the crack front: points A and B (one of them always exhibiting the maximum SIF along the crack front) and an intermediate point. The latter corresponds to the half-length between the points A and B for the case of the embedded cracks (Figure 7a) and is associated with the minimum SIF over the crack front for the surface cracks (Figure 7b) and for the corner-type cracks (Figure 7c). The maximum dimensionless SIF over the crack front is higher in the case of corner cracks, intermediate for surface flaws, and lower for embedded defects. The exponent m of the Paris law makes the SIF decrease for the embedded case, whereas for the case of surface and corner cracks, it makes the SIF increase.

The *embedded cracks* exhibit approximately the same SIF over the crack front, up to a/t ~ 0.4, from which the SIF diminishes continuously along the crack front (from a maximum value in A to a minimum in B). For *surface cracks*, the maximum SIF is achieved at point B (where the crack intersects the surface) and the minimum SIF at an intermediate point in such a manner that the SIF diminishes along the crack front when the point shifts away from the surface and increases along such a front when the point approaches the center. In the case of *corner cracks*, the shallower ones (with small depth) present the maximum SIF at point A (with close values in A and B) and the deeper ones exhibit that maximum SIF at point B. The minimum SIF for these cracks is achieved in an intermediate point over the crack front.

The crack growth rate for the preferential crack path (Figure 8) is higher for the corner configuration than for the surface crack, and higher for the latter than for the embedded defect (in the same conditions). The dimensionless number of cycles n increases with the exponent m of the Paris law. The most dangerous situations are those for plates under tension with corner cracks inside because they exhibit quicker propagation rates and higher maximum SIFs.

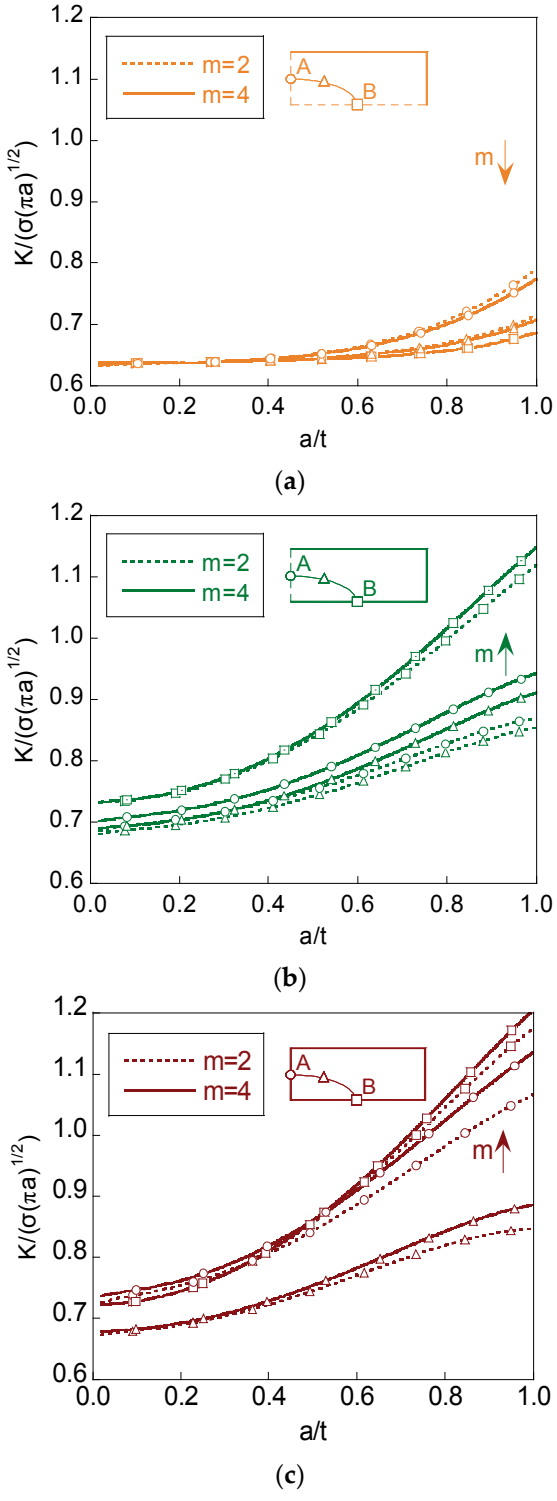

Figure 7. Dimensionless SIFs for the preferential cracking paths given at the A, B, and intermediate points located on the front of a crack of the following types: (**a**) embedded; (**b**) surface; (**c**) corner. (The arrows indicate the direction in which the curves are moved with the increase of the Paris *m* exponent).

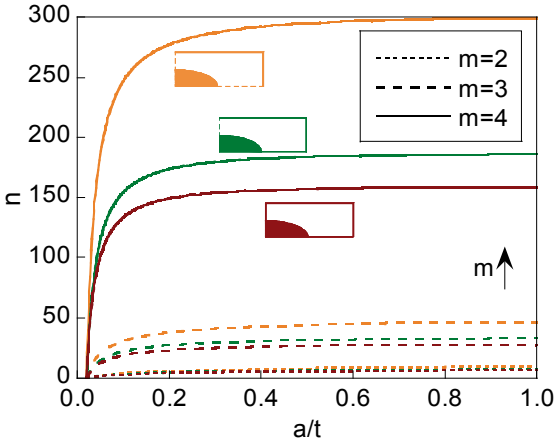

Figure 8. Dimensionless number of cycles for the preferential crack paths. (The arrows indicate the direction in which the curves are moved with the increase of the Paris *m* exponent).

5. Conclusions

Fatigue growth of elliptical-shape cracks in plates subjected to remote tension takes place by approaching a *preferential cracking path* corresponding to a very shallow quasi-circular initial crack. The convergence (closeness between propagation curves starting from different initial geometries) is quicker for surface cracks than for corner ones, and faster for the latter than for embedded ones.

In the matter of the preferential cracking paths:

(i) Those paths associated with embedded cracks exhibit aspect ratios higher than 1 and increase with the crack depth, while they are lower than 1 and diminish with the crack depth in the case of surface and corner cracks.

(ii) Any increase of the Paris exponent of the material leads to a decrease of the aspect ratio in the case of surface and corner cracks and, on the other hand, to an increase of it in the case of embedded flaws.

(iii) Both the crack propagation rate and the maximum stress intensity factor (SIF) are higher for the case of corner cracks than for surface ones, and higher for the latter than for the embedded defects.

Acknowledgments: The authors wish to acknowledge the financial support provided by the following Spanish Institutions: Ministry for Science and Technology (MICYT; Grant MAT2002-01831), Ministry for Education and Science (MEC; Grant BIA2005-08965), Ministry for Science and Innovation (MICINN; Grant BIA2008-06810), Ministry for Economy and Competitiveness (MINECO; Grant BIA2011-27870), and Junta de Castilla y León (JCyL; Grants SA067A05, SA111A07 and SA039A08).

Author Contributions: J.T., J.-C.M., and B.G. conceived and designed the numerical modeling; J.-C.M. developed the computer programs; J.T., J.-C.M., and B.G. analyzed the data; J.T. and B.G. wrote the paper.

Conflicts of Interest: The authors declare no conflict of interest.

Nomenclature

a	crack depth
a_0	initial crack depth
a_f	final crack depth
a/b	crack aspect ratio
$(a/b)_0$	initial crack aspect ratio
a/t	relative crack depth
$(a/t)_0$	initial relative crack depth
Δa_i	crack advance at the point i
Δa(max)	maximum crack advance in the iterations
b	second dimension of the crack (modeled as an ellipse)

C	Paris constant
da/dN	crack growth rate
F	parameter to obtain K
F_i	parameter F to obtain K at the point i
F(max)	maximum parameter F over the crack front
ϕ	angle characterizing a point at the crack front
K	stress intensity factor (SIF)
ΔK	stress intensity factor range
m	Paris exponent
n	dimensionless number of cycles required for fatigue crack propagation
N	number of cycles required for fatigue crack propagation
p	point over the crack front
Q	shape factor
σ	remote tensile stress
$\Delta\sigma$	remote tensile stress range
t	plate thickness
w	plate width
z	number of parts in which each ellipse (crack front) is divided

Appendix A

The SIFs used in the present paper were those obtained by Newman and Raju [1]. The coefficients included in the SIF expressions are as follows, see [1]:

- *For* $\frac{a}{b} \le 1$ *and elliptical embedded crack [1]*

$$M_1 = 1 \tag{A1}$$

$$M_2 = \frac{0.05}{0.11 + (a/b)^{3/2}} \tag{A2}$$

$$M_3 = \frac{0.29}{0.23 + (a/b)^{3/2}} \tag{A3}$$

$$g = 1 - \frac{(a/t)^4 \left[2.6 - 2(a/t)\right]^{1/2}}{1 + 4(a/b)} \left|\cos\phi\right| \tag{A4}$$

$$f_\phi = \left[\left(\frac{a}{b}\right)^2 \cos^2\phi + \sin^2\phi\right]^{1/4} \tag{A5}$$

- *For* $\frac{a}{b} \le 1$ *and semi-elliptical surface crack [1]*

$$M_1 = 1.13 - 0.09\left(\frac{a}{b}\right) \tag{A6}$$

$$M_2 = -0.54 + \frac{0.89}{0.2 + (a/b)} \tag{A7}$$

$$M_3 = 0.5 - \frac{1}{0.65 + (a/b)} + 14\left[1 - \left(\frac{a}{b}\right)\right]^{24} \tag{A8}$$

$$g = 1 + \left[0.1 + 0.35\left(\frac{a}{t}\right)^2 \right]\left(1 - \sin\phi\right)^2 \tag{A9}$$

f_ϕ is given by Equation (A5).

- *For* $\frac{a}{b} \le 1$ *and quarter-elliptical corner crack [1]*

$$M_1 = 1.08 - 0.03\left(\frac{a}{b}\right) \tag{A10}$$

$$M_2 = -0.44 + \frac{1.06}{0.3 + \left(a/b\right)} \tag{A11}$$

$$M_3 = -0.5 + 0.25\left(\frac{a}{b}\right) + 14.8\left[1 - \left(\frac{a}{b}\right)\right]^{15} \tag{A12}$$

$$g = g_1 g_2 \tag{A13}$$

$$g_1 = 1 + \left[0.08 + 0.4\left(\frac{a}{t}\right)^2 \right]\left(1 - \sin\phi\right)^3 \tag{A14}$$

$$g_2 = 1 + \left[0.08 + 0.15\left(\frac{a}{t}\right)^2 \right]\left(1 - \cos\phi\right)^3 \tag{A15}$$

f_ϕ is given by Equation (A5).

- *For* $\frac{a}{b} > 1$ *and elliptical embedded crack [1]*

$$M_1 = \left(\frac{b}{a}\right)^{1/2} \tag{A16}$$

$$f_\phi = \left[\left(\frac{b}{a}\right)^2 \sin^2\phi + \cos^2\phi \right]^{1/4} \tag{A17}$$

M_2, M_3, and g are given by Equations (A2)–(A4).

- *For* $\frac{a}{b} > 1$ *and semi-elliptical surface crack [1]*

$$M_1 = \left(\frac{b}{a}\right)^{1/2}\left[1 + 0.04\left(\frac{b}{a}\right)\right] \tag{A18}$$

$$M_2 = 0.2\left(\frac{b}{a}\right)^4 \tag{A19}$$

$$M_3 = -0.11\left(\frac{b}{a}\right)^4 \tag{A20}$$

$$g = 1 + \left[0.1 + 0.35\left(\frac{b}{a}\right)\left(\frac{a}{t}\right)^2 \right]\left(1 - \sin\phi\right)^2 \quad \text{(A21)}$$

f_ϕ is given by Equation (A17).

- *For* $\frac{a}{b} > 1$ *and quarter-elliptical corner crack [1]*

$$M_1 = \left(\frac{b}{a}\right)^{1/2}\left[1.08 - 0.03\left(\frac{b}{a}\right)\right] \quad \text{(A22)}$$

$$M_2 = 0.375\left(\frac{b}{a}\right)^2 \quad \text{(A23)}$$

$$M_3 = -0.25\left(\frac{b}{a}\right)^2 \quad \text{(A24)}$$

$$g_1 = 1 + \left[0.08 + 0.4\left(\frac{b}{t}\right)^2 \right]\left(1 - \sin\phi\right)^3 \quad \text{(A25)}$$

$$g_2 = 1 + \left[0.08 + 0.15\left(\frac{b}{t}\right)^2 \right]\left(1 - \cos\phi\right)^3 \quad \text{(A26)}$$

g and f_ϕ are given by Equations (A13) and (A17).

References

1. Newman, J.C., Jr.; Raju, I.S. Stress-intensity factor equations for cracks in three-dimensional finite bodies subjected to tension and bending loads. In *Computational Methods in the Mechanics of Fracture*; Atluri, S.N., Ed.; Elsevier Science Publishers: Amsterdam, The Netherlands, 1986; pp. 311–334.
2. Wahab, M.A.; de Roeck, G. A finite element solution for elliptical cracks using the ICCI method. *Eng. Fract. Mech.* **1996**, *53*, 519–526.
3. Le Delliou, P.; Barthelet, B. New stress intensity factor solutions for an elliptical crack in a plate. *Nucl. Eng. Des.* **2007**, *237*, 1395–1405.
4. Peng, Y.; Tong, L.; Zhao, X.-L.; Xiao, Z. Modified stress intensity factor equations for semi-elliptical surface cracks in finite thickness and width plates. *Proc. Eng.* **2011**, *14*, 2601–2608.
5. Newman, J.C., Jr.; Raju, I.S. *Analyses of Surface Cracks in Finite Plates under Tension or Bending Loads*; NASA TP-1578; NASA: Hampton, VA, USA, 1979.
6. Guozhong, C.; Kangda, Z.; Dongdi, W. Analyses of embedded elliptical cracks in finite thickness plates under uniform tension. *Eng. Fract. Mech.* **1996**, *54*, 579–588.
7. Raju, I.S.; Newman, J.C., Jr. *Finite-Element Analysis of Corner Cracks in Rectangular Bars*; NASA TM-89070; NASA: Hampton, VA, USA, 1987.
8. Wu, S. Shape change of surface crack during fatigue growth. *Eng. Fract. Mech.* **1985**, *22*, 897–993.
9. Gilchrist, M.; Smith, R. Finite element modelling of fatigue crack shapes. *Fatigue Fract. Eng. Mater. Struct.* **1991**, *6*, 617–626.
10. Gilchrist, M.; Chipalo, M.; Smith, R. Shape development of surface defects in tension fatigued finite thickness plates. *Int. J. Press. Vessels Pip.* **1992**, *49*, 121–137.
11. Nykänen, T. Fatigue crack growth simulations based on free front shape development. *Fatigue Fract. Eng. Mater. Struct.* **1996**, *19*, 99–109.
12. Wu, Z. The shape of a surface crack in a plate based on a given stress intensity factor distribution. *Int. J. Press. Vessels Pip.* **2006**, *83*, 168–180.
13. Toribio, J.; Matos, J.C.; González, B. Aspect ratio evolution associated with surface cracks in sheets subjected to fatigue. *Int. J. Fatigue* **2016**, *92*, 588–595.

14. Paris, P.C.; Erdogan, F. A critical analysis of crack propagation laws. *J. Basic Eng.* **1963**, *85D*, 528–534.
15. Newman, J.C., Jr.; Raju, I.S. Prediction of fatigue crack-growth patterns and lives in three-dimensional cracked bodies. In: *Advances in Fracture Research*; Valluri, S.R., Ed.; Elsevier Science Publishers: New Delhi, India, 1984; pp. 1597–1608.
16. Brennan, F.P.; Ngiam, S.S.; Lee, C.W. An experimental and analytical study of fatigue crack shape control by cold working. *Eng. Fract. Mech.* **2008**, *75*, 355–363.
17. Liu, C.; Chu, S. Prediction of shape change of corner crack by fatigue crack growth circles. *Int. J. Fatigue* **2015**, *75*, 80–88.
18. Branco, R.; Antunes, F.V.; Costa, J.D. A review on 3D-FE adaptive remeshing techniques for crack growth modelling. *Eng. Fract. Mech.* **2015**, *141*, 170–195.
19. Lin, X.B.; Smith, R.A. Finite element modelling of fatigue crack growth of surface cracked plates: Part III: Stress intensity factor and fatigue crack growth life. *Eng. Fract. Mech.* **1999**, *63*, 541–556.
20. Boukharouba, T.; Pluvinage, G. Prediction of semi-elliptical defect form, case of a pipe subjected to internal pressure. *Nucl. Eng. Des.* **1999**, *188*, 161–171.
21. Gdoutos, E.E.; Hatzitrifon, N. Growth of three-dimensional cracks in finite-thickness plates. *Eng. Fract. Mech.* **1987**, *26*, 883–895.
22. Tan, P.W.; Newman, J.C., Jr.; Bigelow, C.A. Three-dimensional finite-element analyses of corner cracks at stress concentrations. *Eng. Fract. Mech.* **1996**, *55*, 505–512.
23. Shivakumar, K.N.; Newman, J.C., Jr. Stress intensity factors for large aspect ratio surface and corner cracks at a semi-circular notch in a tension specimen. *Eng. Fract. Mech.* **1991**, *38*, 467–473.
24. Lin, X.B.; Smith, R.A. Stress intensity factors for corner cracks emanating from fastener holes under tension. *Eng. Fract. Mech.* **1999**, *62*, 535–553.
25. Mahmoud, M.A.; Hosseini, A. Assessment of stress intensity factor and aspect ratio variability of surface cracks in bending plates. *Eng. Fract. Mech.* **1986**, *24*, 207–221.
26. Toribio, J.; Matos, J.C.; González, B.; Escuadra, J. An automated procedure for the geometrical modelling of a surface crack front. *Struct. Durab. Health Monit.* **2009**, *123*, 1–16.
27. Lin, X.B.; Smith, R.A. An improved numerical technique for simulating the growth of planar fatigue cracks. *Fatigue Fract. Eng. Mater. Struct.* **1997**, *20*, 1363–1373.